GEOPHYSICS, VOL. 69, NO. 1 (JANUARY-FEBRUARY 2004); P. 140–151, 11 FIGS., 2 TABLES.
10.1190/1.1649382

Downloaded 06/29/16 to 178.250.250.21. Redistribution subject to SEG license or copyright; see Terms of Use at http://library.seg.org/

Numerical analysis of near-borehole and anisotropic layer effects on the response of multicomponent induction logging tools

Michael J. Tompkins*, David L. Alumbaugh,‡ Darrell T. Stanley,** and Xinyou Lu§

ABSTRACT

We present finite-difference simulation results that lend new insight into the behavior of multicomponent induction logging tools when in the presence of anisotropic layers, boreholes, and invasion zones. We use four independent models to investigate multicomponent tool properties as well as typical magnetic field responses. In addition, model variations with respect to formation dip angle, layer geometry, and conductivity provide data about the effects of geological variation on the multicomponent responses. Simulations suggest a coaxial tool configuration senses a depth of twice the source–receiver offset, although this depth is reduced to the source–receiver offset with coplanar configurations. Numerical responses in the presence of transversely isotropic layers provide evidence that anisotropy can have a measurable effect on both coaxial and coplanar magnetic fields; these effects increase as layer dip increases. Sensitivity analyses substantiate these numerical results. An investigation of tool responses to varying borehole and invasion zone conductivities and diameters demonstrates that the coplanar tool orientation is much more sensitive to near-borehole variations than the coaxial configuration. A frequency-differencing technique is presented to mitigate unwanted borehole-induced bias in multicomponent data; however, drawbacks include decreased signal strength and possible geological signal destruction.

INTRODUCTION

Electromagnetic (EM) induction logging procedures are standard accompaniments to well drilling for determining near-borehole rock properties, including porosity, oil–water saturation, and fracture location. Typically, EM induction measurements are made using a downhole coaxial magnetic field source and receiver (Figure 1). This configuration allows, at best, an isotropic 2D analysis of formation properties when assuming cylindrical symmetry about a vertical axis. With the advent of induction imaging tools, which utilize multicomponent magnetic field receivers and transaxial transmitters, 3D analysis of EM induction data is possible. Multicomponent analysis of formation electrical properties is especially important for deviated wellbores or anisotropic conditions because the cylindrical geometry often assumed in coaxial induction logging does not exist.

Several studies investigate geological or tool configuration effects on multicomponent logging data. Alumbaugh and Wilt (1998, 2001) analyze magnetic field sensitivities in isotropic media and have published the first results of multicomponent borehole EM modeling. Cheryauka et al. (2001) use an integral equation approach to determine the sensitivity of multicomponent tools to layered formations. They present data as a function of layer dip and discuss thin conductor resolution but do not include effects of anisotropy.

Others have investigated the response of triaxial source–receiver configurations in anisotropic media. For example, Kriegshauser et al. (2000) present data from a new multicomponent logging tool in electrically anisotropic formations but do not concentrate on modeling geologic variations. Lu and Alumbaugh (2001) discuss the distortion of multicomponent sensitivities in an anisotropic whole space using a tensor Green's function approach. Newman and Alumbaugh (2002) and Avdeev et al. (2002) use finite-difference and integral equation solutions to model the multicomponent response in uniaxially anisotropic media; however, they focus on the computational method and validation rather than geological variations and tool specifications. In terms of modeling realistic geological formations, Wang and Fang (2001) use a finite-difference solution to model induction logging responses in 2D anisotropic media with and without a borehole but do not discuss specific

Manuscript received by the Editor August 14, 2002; revised manuscript received May 21, 2003.
*Formerly University of Wisconsin–Madison, Madison, Wisconsin 53706; presently BP America Inc., 501 Westlake Park Blvd., Houston, Texas 77079. E-mail: geofizx2003@yahoo.com.
‡University of Wisconsin–Madison, 2228 Engineering Hall, 1415 Engineering Drive, Madison, Wisconsin 53706. E-mail: alumbaugh@engr.wisc.edu.
**BP America Inc., 501 Westlake Park Blvd., Houston, Texas 77079. E-mail: darrell.stanley@bp.com.
§ExxonMobil Upstream Research Company, P.O. Box 2189, Houston, Texas 77252. E-mail: xinyou.lu@exxonmobil.com.
© 2004 Society of Exploration Geophysicists. All rights reserved.

Downloaded 06/29/16 to 178.250.250.21. Redistribution subject to SEG license or copyright; see Terms of Use at http://library.seg.org/

effects of source geometry, borehole diameter and conductivity, or depth sensitivity.

As an extension of previous work, we model variations in measurement parameters and geologic factors that affect multicomponent induction responses. Source–receiver configurations (e.g., tool offset and source size), layer dip angle, borehole conductivity, borehole diameter, and formation anisotropy are all important factors controlling multicomponent induction logging responses. To isolate these factors and illuminate their effects on individual tool configuration responses and the detection of thin conducting bodies, we provide results from a variety of numerical simulations. Thin fractures, which are modeled as thin anisotropic layers (1 m), and near-borehole conductivity variations are commonly encountered and represent scenarios of interest to the geothermal energy and oil and gas exploration industries.

To simulate multicomponent measurements, we use the iterative finite-difference scheme developed by Newman and Alumbaugh (1995). This isotropic 3D frequency-domain algorithm solves for scattered EM fields and gives accurate simulated induction log responses. We also use the anisotropic finite-difference algorithm presented by Newman and Alumbaugh (2002) to simulate the response in anisotropic fractures or layers. Both schemes solve the electric field vector Helmholtz equation using an implicit scheme based on a Yee staggered-grid solution (Yee, 1966). Unless otherwise stated, our tolerance for numerical error is approximately 1% based on the estimated accuracy of the numerical codes. That is, the finite-difference solutions for the total quadrature fields agree to within 1% of analytical solutions computed with two separate algorithms. We use an isotropic 1D analytical algorithm provided by Ki Ha Lee at Lawrence Berkeley Laboratories and an anisotropic 1D algorithm developed at the University of Wisconsin–Madison (Tompkins, 2003) for numerical verifications.

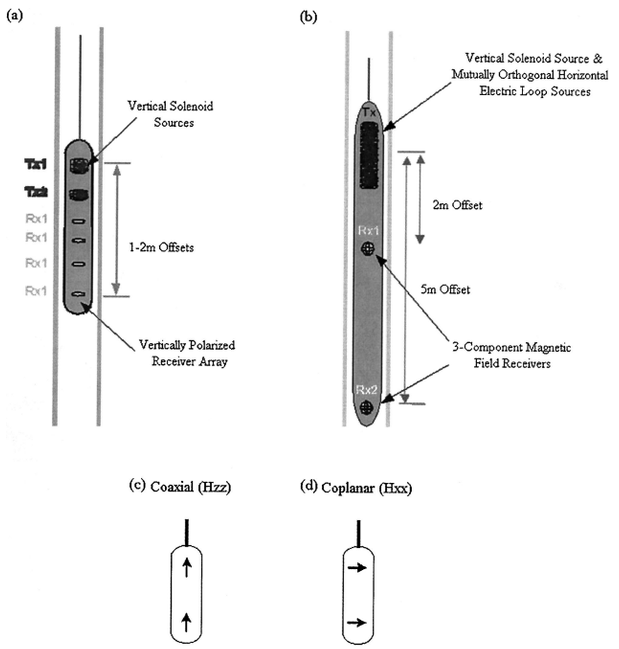

FIG. 1. (a) Schematic of a typical coaxial induction logging tool. (b) Schematic of the three-component long-offset logging tool developed by EMI Inc. (c,d) The two multicomponent source–receiver configurations used in the simulations.

SIMULATED TOOL SPECIFICATIONS

Because this numerical modeling study is designed to give insight specific to multicomponent induction tools, we simulate three-component magnetic field sources and receivers as shown in Figure 1. The simulated tool consists of two mutually orthogonal, horizontally polarized electric loop sources (dimensions: 0.08×1 m) and a vertical solenoid source (dimension: 1 m). The sonde also contains two three-component receivers at two offsets: 2 and 5 m. Source geometries and offsets are chosen based on the GeoBILT tool developed by EMI Inc., as this is one of only two such multicomponent instruments in use. Source magnetic fields are generated at five frequencies between 2 and 40 kHz. At these low frequencies and offsets, the tool is considered to be working in a low-induction-number ($L \leq 1$) regime, where

$$L = \sigma_b \omega \mu l^2. \tag{1}$$

Here, σ_b is electrical conductivity, ω is angular frequency, μ is magnetic permeability and l is source–receiver separation. Under this condition, the magnetic field response is linearly proportional to frequency and conductivity. Also at these frequencies, $\omega\mu\sigma_b \gg \omega^2\mu\varepsilon$, where μ is magnetic permeability and ε is dielectric permittivity. For this condition, propagation is dominantly diffusive and is considered to be dependent primarily on the conductivity of the medium (see Ward and Hohmann, 1988, 135–137). As such, we only consider model conductivity variations in our simulations.

We can combine the three-component sources and receivers to obtain nine tool configurations for measurements in 3D fully anisotropic media. Of these nine components, we include results for the coaxial (H_{zz}) and coplanar (H_{xx} and H_{yy}) configurations (Figure 1). These fully coupled components produce the largest quadrature magnetic field amplitudes recorded in multicomponent logging. Although we realize that null-coupled components must be recorded to recover 3D or anisotropic electrical structures, we exclude these components from our simulations for brevity. Also, given that both coplanar configurations produce similar responses for our simulations, we omit the coplanar y-polarized configuration from our discussion. In all results, total-quadrature magnetic field amplitudes are presented, since these are commonly recorded in the field. The quadrature components are also much more sensitive to conductivity contrasts than the real components, since real components are dominated by the primary field response.

INVESTIGATION DEPTH

Thin conductor models

Here, we simulate multicomponent responses to 1-m-thick half-infinite conductors terminated at varying lateral depths from the borehole axis (Figure 2a). The 2D conductors are extended in the x-direction beyond the borehole axis by 0.25, 2, 4, 6, 7.5, and 10 m. A model containing a conductor with infinite extent in the x-direction is also included. The horizontal conducting layer, in all cases, is transversely isotropic, with the horizontal conductivity being five times the vertical (Figure 2a). We model the coaxial and coplanar responses for

Downloaded 06/29/16 to 178.250.250.21. Redistribution subject to SEG license or copyright; see Terms of Use at http://library.seg.org/

both 2- and 5-m source–receiver offsets. The simulated tool axis is vertical, with source and receivers positioned at $x = y = 0$. Simulated data measurements were made every 0.5 m across the model space in the $+z$-direction. Since the estimated accuracy of our simulations is 1%, differences less than this are considered numerical noise.

Simulation results

The depth to which typical coaxial induction logging tools are sensitive to near-borehole properties is approximately twice the source–receiver separation based on the work of Moran (1982). Alumbaugh and Wilt (2001) extend Moran's work to include isotropic whole-space sensitivities for the source–receiver configurations used here. We present results that investigate these depth sensitivities in the presence of an anisotropic thin conductor. While our results do not include noise effects, they may be used to estimate the relative depth penetration of different tool configurations. The results are plotted in Figures 3 and 4 and demonstrate that depth sensitivity is dependent on both source–receiver offset and polarization.

As predicted by Moran (1982) for coaxial configurations, the investigation depth is approximately twice the source–receiver separation. This is evident in Figure 3a, where the difference between the coaxial responses at 4 and 6 m is ~1% and nearly zero when the conductor is extended to 10 m beyond the tool axis. A similar result is shown in Figure 3b, where the sensitivity depth is increased to 10 m with a 5-m source–receiver offset. The coplanar responses are plotted in Figures 4a and 4b and demonstrate a contrasting result. In this case, the coplanar response is sensitive to a depth of approximately one source–receiver offset. This result is expected, since the whole-space sensitivities for this configuration are more focused near the borehole

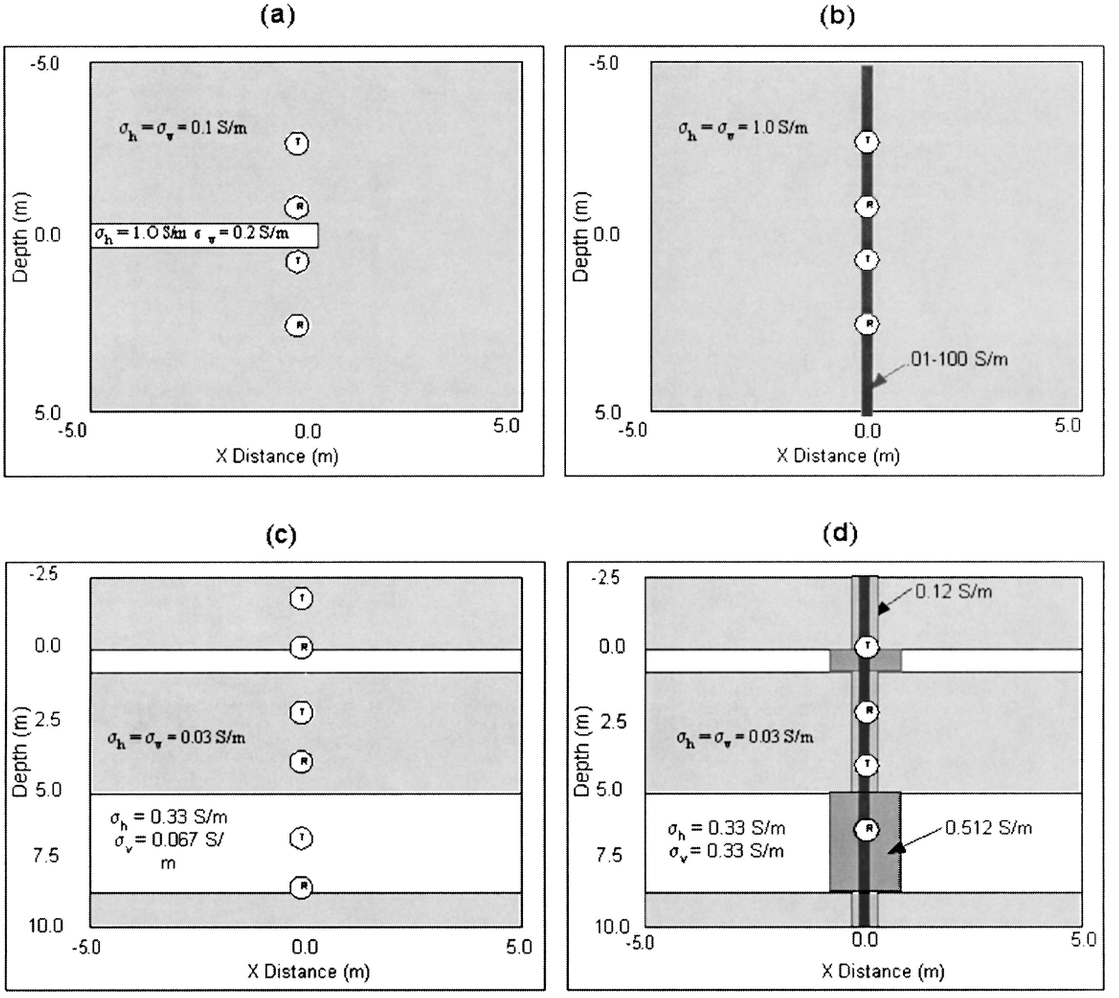

FIG. 2. Cross-sections of the four 3D models used in the numerical simulations. Example source and receiver locations are denoted by T and R, respectively. (a) The half-infinite fracture model used to determine relative depth sensitivity. The lateral extent of the fracture away from the tool axis is varied from 0.25 m to infinity. (b) Whole-space model containing a conductive borehole. Borehole conductivities range from 0.01 to 100 S/m, while borehole diameters range from 0.1 to 0.4 m. (c) Five-layer model adapted from Wang and Fang (2001). Horizontal layering is shown, but dipping layers (60°) are also simulated. (d) The same model as in (c) with isotropic conductivities and the addition of a vertical borehole and invasion zone. The borehole diameter is 0.2 m; the invasion zone diameter varies between 0.8 and 1.6 m in the resistive and conductive layers, respectively.

Downloaded 06/29/16 to 178.250.250.21. Redistribution subject to SEG license or copyright; see Terms of Use at http://library.seg.org/

than for the coaxial configuration (Figures 5c and 5d). Alumbaugh and Wilt (2001) also demonstrate that geometric effects in addition to S/N considerations limit the effective imaging depth to approximately twice the source–receiver offset for coaxial configurations but less for coplanar configurations. Both the 2- and 5-m coplanar source–receiver configurations show this diminished depth sensitivity.

BOREHOLE EFFECTS

The sensitivity for the coaxial configuration is minimized along the borehole axis (Figure 5a); therefore, the borehole effect is expected to be minimal (Alumbaugh and Wilt, 2001). The coplanar configuration, however, exhibits sensitivity that is maximized along the borehole axis (Figures 5c and 5d). Thus, the borehole may contribute considerably to the coplanar response. Here, we investigate the effect of a borehole of variable diameter and conductivity for both coaxial and coplanar source–receiver configurations. The resulting effect, termed borehole-induced bias, is distinguished from the more general term noise because the borehole-induced bias results from a determinable response.

The borehole-induced bias is determined for each model by comparing the total and primary quadrature components of the magnetic field, expressed as a percentage. Here, the primary field is the entire magnetic field that would be recorded in the absence of a borehole, and the total field is the response from the borehole conductivity contrasts and background. In essence, any difference between the primary and total quadrature fields is attributable to the borehole only. To determine percent differences, we evaluate the equality:

$$\text{error}(\%) = \left[\frac{(QH_p - QH_t)}{QH_p}\right] \times 100. \qquad (2)$$

Here, QH_p is the quadrature component of the primary field (i.e., the formation response we wish to recover) and QH_t is the quadrature component of the total field. The percent difference between the primary and total quadrature fields is calculated at each frequency as a function of source–receiver offset.

Borehole models

Models consist of a 3D grid with a cylindrical borehole aligned parallel to the z-axis and located at $x = y = 0$

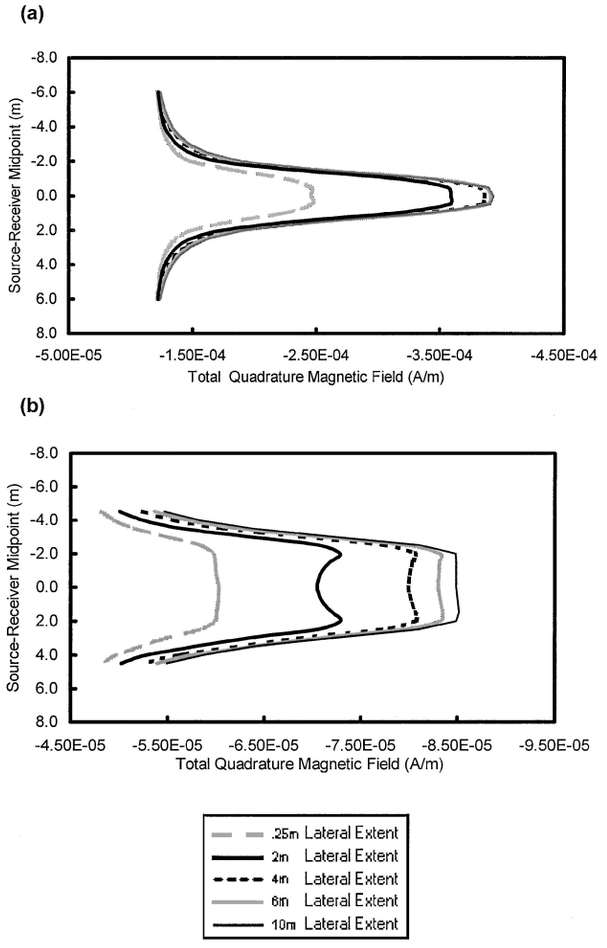

FIG. 3. Simulated coaxial data for the half-infinite conductor model shown in Figure 2a. (a) Coaxial data at 2 m source–receiver offset. (b) Coaxial data at 5 m offset.

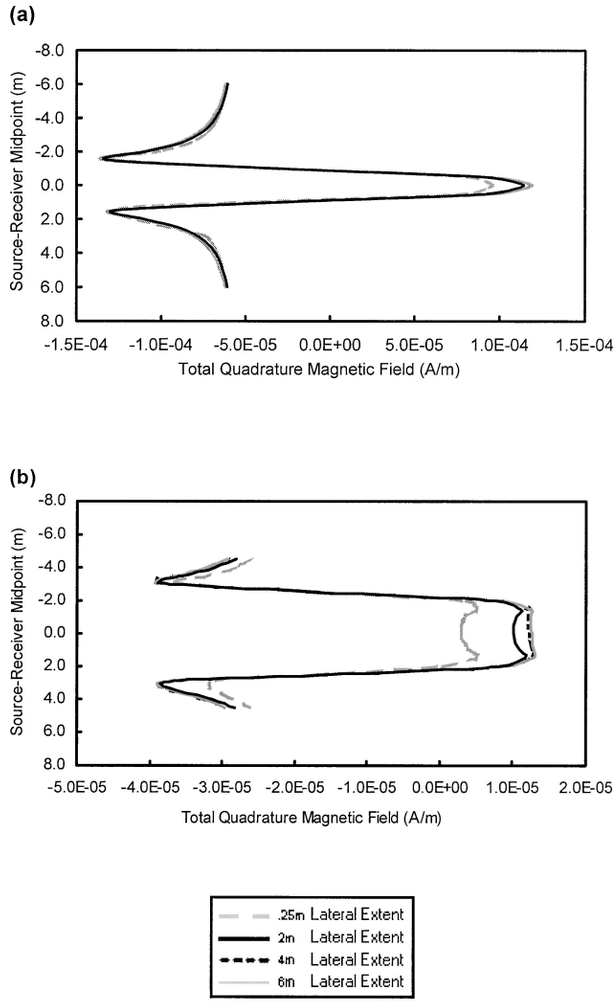

FIG. 4. Simulated coplanar data for the half-infinite conductor model shown in Figure 2a. (a) Coplanar data at 2 m source–receiver offset. (b) Coplanar data at 5 m offset.

Downloaded 06/29/16 to 178.250.250.21. Redistribution subject to SEG license or copyright; see Terms of Use at http://library.seg.org/

(Figure 2b). The borehole extends through the entire model space in the z-direction. A 3D rectangular grid adequately represents a cylindrical borehole, provided the node spacing is small enough in relation to the borehole diameter (Newman and Alumbaugh, 2002). In all cases, the source is located at $x = y = 0$ and $z = 5$ m. Nine receivers are located directly below the source, the first one at 1.0 m away and the rest at 0.5-m increments from the source in the $+z$ direction, resulting in a 5-m-long source–receiver array. For all coaxial simulations, a 1-m-long solenoid source is used. In the finite-difference algorithm, the 1-m source is simulated by integrating a series of magnetic dipoles along the axis of the tool. This source has no width in the x- or y-direction. This is not problematic, since the source–receiver separations of interest, 1–5 m, are much greater than the radius of the true source (~2 cm). The coplanar source consists of a rectangular loop, 1×0.08 m, with the long dimension parallel to the tool axis. The loop source is oriented with its moment in the $+x$-direction.

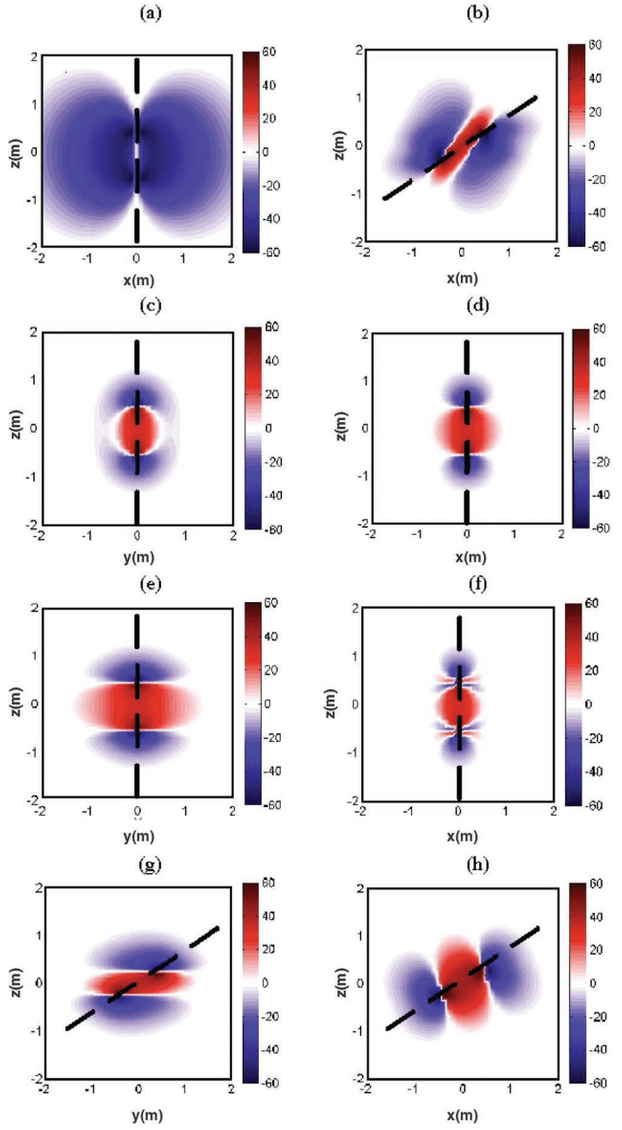

FIG. 5. Logarithmically normalized multicomponent sensitivities as a function of position in homogeneous isotropic and anisotropic whole spaces. Views represent 2D plane sections of 3D sensitivities for quadrature magnetic fields. Dotted lines indicate formation dip angle. Anisotropic sensitivities represent formations with an anisotropy coefficient of $\lambda = \sqrt{\sigma_h/\sigma_v} = \sqrt{10}$. (a) Coaxial sensitivity in the $y = 0$ plane for both anisotropic and isotropic media. (b) Coaxial sensitivity in the $y = 0$ plane for dipping (60°) anisotropic media. (c) Coplanar sensitivity in the $x = 0$ plane for isotropic media. (d) Coplanar sensitivity in the $y = 0$ plane for isotropic media. (e) Coplanar sensitivity in the $x = 0$ plane for anisotropic media. (f) Coplanar sensitivity in the $y = 0$ plane for anisotropic media. (g) Coplanar sensitivity in the $x = 0$ plane for dipping (60°) anisotropic media. (h) Coplanar sensitivity in the $y = 0$ plane for dipping (60°) anisotropic media.

The accuracy of the 3D algorithm for simulating coaxial responses to these types of borehole models is evaluated by comparing results with analytic solutions provided by Ki Ha Lee at Lawrence Berkeley National Labs. Total-quadrature magnetic field amplitudes for the independent simulations differ by no more than 2% in nearly all cases. One exception is for large-diameter (0.4 m) borehole results where amplitudes differ by 1–5% at offsets less than 3 m.

Berthold Kriegshauser of Baker Atlas provided analytic coplanar results for a 10-S/m, 0.1-m-diameter borehole in a 1-S/m background. Again, agreement is quite good with results differing by less than 2% at all but one source–receiver offset (3.5 m @20 kHz) where it is 4.5%. This larger error is because of a total quadrature magnetic field zero crossing between 3 and 4 m offset in the finite-difference results.

Simulation results

Variable borehole conductivity.—First, we evaluate the effect of variable borehole conductivities on the tool response, the borehole-induced bias. Models consist of 0.1-m-diameter boreholes in a homogeneous 1.0-S/m background. Mud resistivity values are 0.01, 0.1, 10, and 100 S/m. The coaxial magnetic field results are shown in Figure 6a. Although the amplitudes are nearly identical for the primary and total fields when the borehole conductivity is less than 0.1 S/m, there are measurable differences in the responses when the borehole conductivity is increased. In addition, the magnitude of the borehole-induced bias is similar for both 2- and 20-kHz source frequencies, with the percent difference values for 20 kHz being only slightly larger. Values of percent differences are shown in Table 1 for various offsets and conductivities. At 2- and 5-m offsets, the differences are small but are greater than zero for 0.01-, 0.1-, and 10-S/m boreholes. The 100-S/m borehole model produces the largest discrepancy, with percent difference values ranging from −7.6% at 2 m offset to −1.3% at 5 m offset.

The results for the coplanar configuration at 2 and 20 kHz are shown in Figure 6b. Similar to the coaxial results, the amplitude of the quadrature component of the primary field decreases with increasing offset. In addition, the percent differences between the primary and total fields decrease with decreasing borehole conductivity. The less conductive boreholes, 0.01 and 0.1 S/m, have percent differences that range from −1.5% to −6.8% at 2 m offset and from −0.5% to −3.2% at 5 m offset (Table 1). As with the coaxial results, the 100-S/m borehole produces the largest coplanar percent difference values, which reduce from 9.7% to 24.8% at 2 m offset to 2.2% to 8.5% at 5 m offset. Also, the borehole-induced bias appears to be less

Downloaded 06/29/16 to 178.250.250.21. Redistribution subject to SEG license or copyright; see Terms of Use at http://library.seg.org/

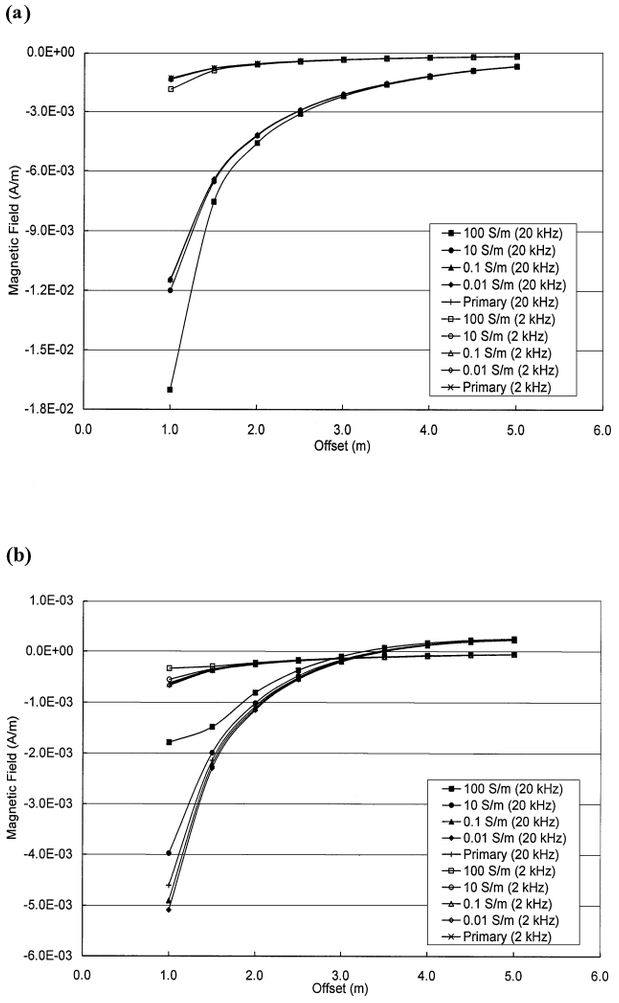

FIG. 6. Variable-conductivity borehole simulation results. The total-quadrature magnetic fields are presented at variable offsets ranging from 1.0 to 5.0 m. Results are also presented for both 2- and 20-kHz source frequency. (a) Coaxial configuration. (b) Coplanar configuration.

dependent on frequency than conductivity (Table 1). One exception is the coplanar response to the 100-S/m borehole at 20 kHz. In this case, the borehole-induced bias is as much as 8.5 times greater at 20 kHz than at 2 kHz. Unlike the coaxial responses, there is a zero crossing between 3.0 and 3.5 m for the 20-kHz results. This zero crossing contributes to larger percent differences for the coplanar data. As described before, the borehole-induced bias is larger for the coplanar data, since this configuration has a sensitivity that is focused near the source–receiver and borehole axis.

Variable borehole diameter.—Here we examine how varying the borehole diameter affects the multicomponent response. We include simulations for three borehole diameters: 0.1, 0.2, and 0.4 m (Figures 7a and b). Each model consists of a 10.0-S/m borehole in a 1.0-S/m background. The 0.1-m model is identical to the 10-S/m case from the variable borehole conductivity analysis.

The magnetic field results for the coaxial configuration are shown in Figure 7a. As was apparent from the variable conductivity simulations, percent differences decrease with increasing offset for all cases. Values of percent differences also increase with increasing borehole diameter, although they are relatively constant with frequency (Table 2). At 2 m offset, percent difference values increase from −0.7% for a 0.1-m borehole to −15.2% for a 0.4-m borehole. Values are smaller at 5 m offset, ranging from 0.1% for a 0.1-m borehole to −2.5% for a 0.4-m borehole.

The results for the coplanar configuration are shown in Figure 7b. Again, percent difference values decrease with increasing offset and increase with increasing diameter (Table 2). These values are also significantly lower for 2 kHz than for 20 kHz. At 2 kHz, values of percent differences at 2 m increase from 2.5% to 26.8% for 0.1- to 0.4-m-diameter boreholes, while at 5 m offset the increase is from 0.8% to 8.5%. At 20 kHz, values increase from 6.0% to 67.2% for 0.1- to 0.4-m-diameter boreholes and from −2.0% to −24.9% at 5 m offset. The 20-kHz data have the same zero crossing evident in the variable conductivity results at 3.5 m, while the zero crossing shown in Figure 7b moves to shorter source–receiver

Table 1. Percent differences between primary and total quadrature magnetic field amplitudes for variable-conductivity borehole simulations. The differences are computed using equation (2) in the text.

Borehole conductivity (S/m)	Configuration	Frequency (kHz)	Percent difference at various offsets (m)				
			1.00	2.00	3.00	4.00	5.00
0.01	H_{zz}	2	0.5	0.1	0.0	0.0	0.0
0.01	H_{zz}	20	0.5	0.1	0.0	0.0	0.0
0.1	H_{zz}	2	0.4	0.1	0.0	0.0	0.0
0.1	H_{zz}	20	0.5	0.1	0.0	0.0	0.0
10	H_{zz}	2	−3.9	−0.7	−0.3	−0.2	−0.1
10	H_{zz}	20	−4.4	−0.9	−0.4	−0.2	−0.1
100	H_{zz}	2	−42.6	−7.6	−3.4	−2.0	−1.3
100	H_{zz}	20	−48.1	−9.7	−4.6	−2.7	−1.6
0.01	H_{xx}	2	−8.3	−4.3	−3.5	−3.3	−3.1
0.01	H_{xx}	20	−10.4	−6.8	−10.6	2.6	−1.1
0.1	H_{xx}	2	−4.8	−1.5	−0.9	−0.6	−0.5
0.1	H_{xx}	20	−6.4	−3.5	−6.6	4.2	1.1
10	H_{xx}	2	10.3	2.5	1.4	1.0	0.8
10	H_{xx}	20	13.8	6.0	11.2	−7.1	−2.0
100	H_{xx}	2	45.6	9.7	5.5	5.8	2.2
100	H_{xx}	20	61.3	24.8	46.5	−30.2	−8.5

offsets with increasing borehole diameter. The 20-kHz data for the 0.4-m-diameter borehole include a second zero crossing at 1 m offset, which is a direct consequence of borehole size. At 20 kHz, the 0.4-m-diameter borehole is large enough that the simulated coplanar tool senses only the conductive borehole itself. As a result, the total field response approximates that which would be recorded for the primary field in a conductive whole space. A similar result is not recorded for the 2-kHz simulation since the response is an order of magnitude smaller than the response at 20 kHz.

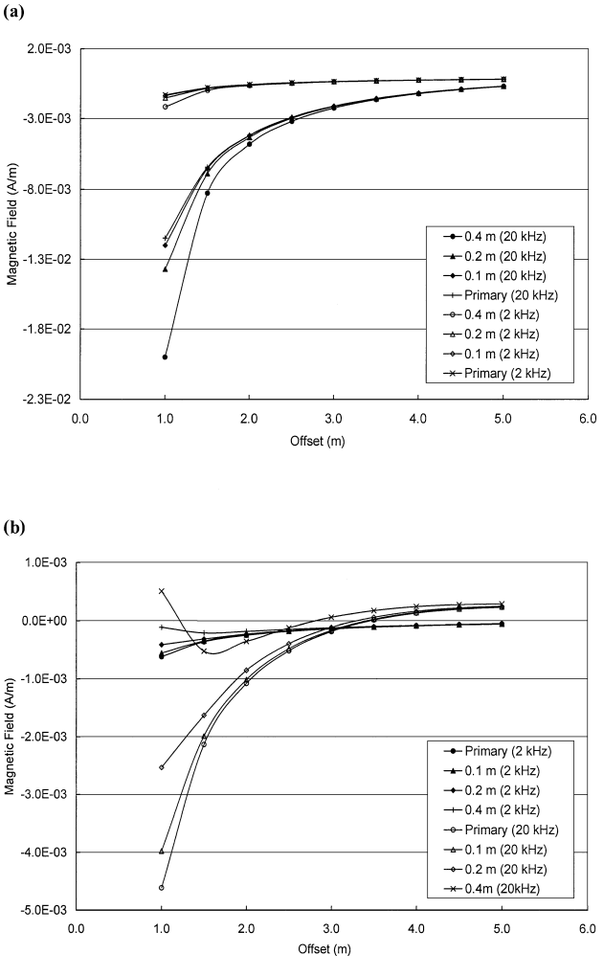

FIG. 7. Variable-diameter borehole simulation results. The total-quadrature magnetic fields are presented at variable offsets ranging from 1.0 to 5.0 m. Results are also presented for both 2- and 20-kHz source frequency. (a) H_{zz} (coaxial) configuration. (b) H_{xx} (coplanar) configuration.

These results indicate that the borehole-induced bias decreases with increasing source–receiver offset, increases only slightly with increasing frequency, and increases with increasing borehole diameter. As mentioned before, the borehole-induced bias is larger for the coplanar configuration and is significant for the 0.4-m diameter borehole to offsets as large as 5 m.

ANISOTROPIC LAYERING EFFECTS

Here, the simulations consist of a more realistic five-layer system. The model follows that presented by Wang and Fang (2001) and is shown in Figure 2c. The layers are infinite in both the x- and y-planes. For both the isotropic and anisotropic simulations, the background conductivity is 0.02 S/m. In the isotropic simulations the conducting layer values are 0.33 S/m. For the anisotropic models, the horizontal conductivity of the layers is 0.33 S/m; the vertical conductivity is 0.067 S/m. Results are presented in Figures 8 and 9 for the horizontally layered model shown in Figure 2c as well as for a model where the five layers dip at 60^o to a vertical borehole axis. The numerical results for these simulations are compared with analytical solutions and are computed using the anisotropic 1D algorithm described in the introduction; they show good agreement. For reference, the anisotropic analytical solutions are plotted with the numerical data in Figures 8 and 9.

Dipping-layer results

Isotropic and anisotropic results are presented in Figure 8 for the coaxial configuration. At 0° dip, the computed total magnetic fields are equal for both the anisotropic and isotropic cases, even though the layers have different vertical conductivities. This is because the coaxial configuration is sensitive only to the horizontal component of the anisotropic conductivity, which is identical to the isotropic case. In contrast, the coaxial response at 60° yields smaller total field amplitudes for the anisotropic model (Figure 8b). This is explained by the

Table 2. Percent differences between primary and total quadrature magnetic field amplitudes for variable-diameter borehole simulations. The differences are computed using equation (2) in the text.

Borehole diameter (m)	Configuration	Frequency (kHz)	Percent difference at various offsets (m)				
			1.00	2.00	3.00	4.00	5.00
0.1	H_{zz}	2	−3.9	−0.7	−0.3	−0.2	−0.1
0.1	H_{zz}	20	−4.4	−0.9	−0.4	−0.2	−0.1
0.2	H_{zz}	2	−17.0	−2.9	−1.3	−0.7	−0.5
0.2	H_{zz}	20	−19.3	−3.7	−1.8	−1.0	−0.6
0.4	H_{zz}	2	−65.6	−11.9	−5.2	−3.0	−2.0
0.4	H_{zz}	20	−74.1	−15.2	−7.0	−4.0	−2.5
0.1	H_{xx}	2	10.3	2.5	1.4	1.0	0.8
0.1	H_{xx}	20	13.8	6.0	11.2	−7.1	−2.0
0.2	H_{xx}	2	33.5	8.6	4.9	3.5	3.0
0.2	H_{xx}	20	45.1	20.8	39.6	−25.6	−7.2
0.4	H_{xx}	2	82.0	26.8	15.4	8.5	8.5
0.4	H_{xx}	20	111.0	67.2	131.2	−86.8	−24.9

Downloaded 06/29/16 to 178.250.250.21. Redistribution subject to SEG license or copyright; see Terms of Use at http://library.seg.org/

decrease in effective horizontal conductivity resulting from the layer dip. If we consider the effective conductor width, which the tool senses, it is evident that as we increase the dip of the layers, the horizontal layer width decreases as 1/sin of the dip angle. The coaxial configuration is sensitive, or coupled, only to the horizontal conductivity of the medium, so we expect the coaxial amplitude to decrease as the horizontal component of layer width decreases with dip. The amplitude decrease with dip is also, in large part, the result of a sensitivity sign change at high dip angles. As shown in Figure 5, when the angle between the tool and formation is increased to 60°, the effects of anisotropy become pronounced. For the coaxial configuration,

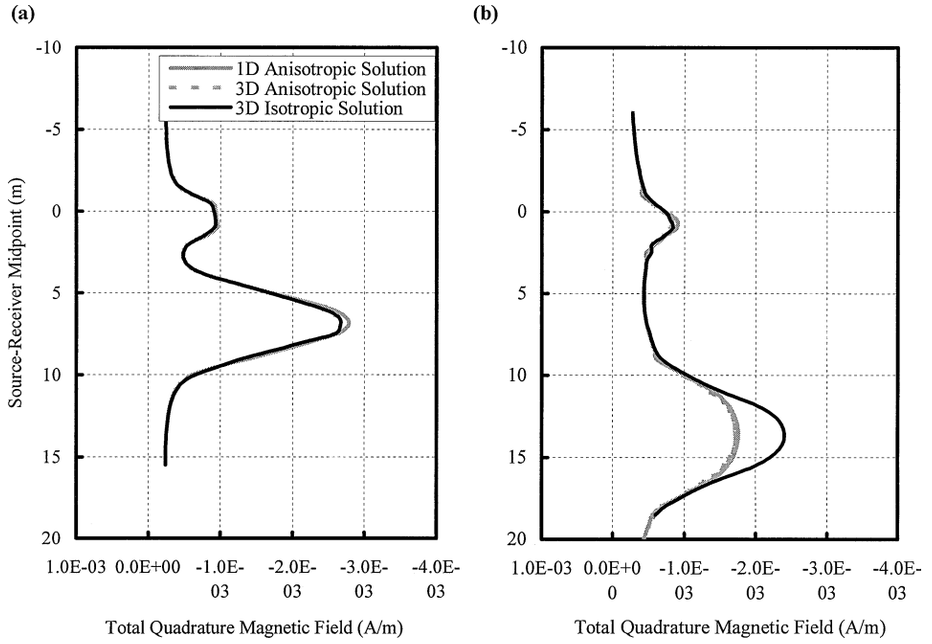

FIG. 8. Coaxial responses for the five-layer model shown in Figure 2c. The 1D analytical solutions for the anisotropic case are provided along with the 3D finite-difference results. (a) Response for the five-layer anisotropic model at 0° dip. The anisotropic and isotropic numerical results are identical for this model. (b) Response for the five-layer anisotropic model at 60° dip.

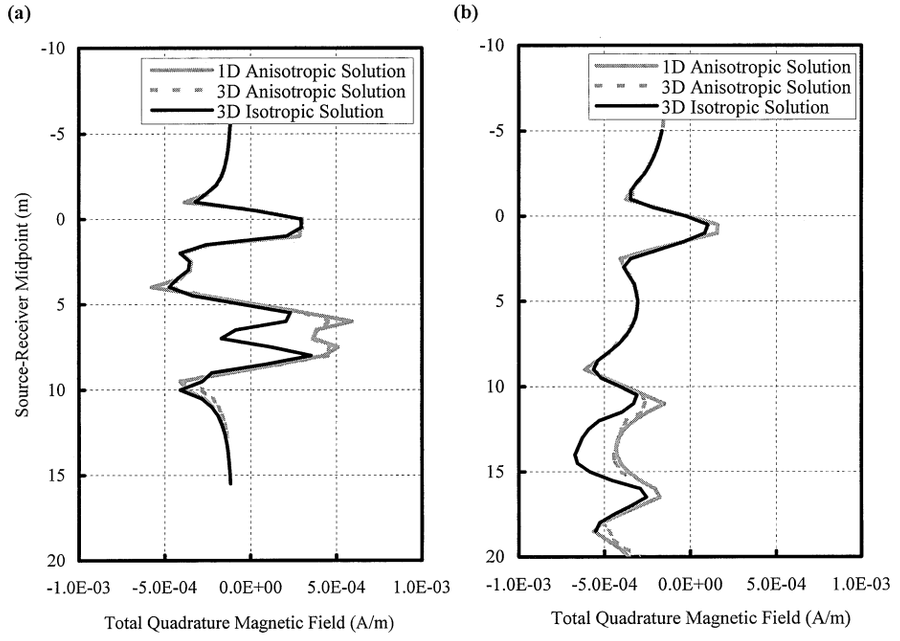

FIG. 9. Coplanar responses for the five-layer model shown in Figure 2c. The 1D analytical solutions for the anisotropic cases are provided along with the 3D finite-difference results. (a) Response for the five-layer anisotropic model at 0° dip. (b) Response for the five-layer anisotropic model at 60° dip.

Downloaded 06/29/16 to 178.250.250.21. Redistribution subject to SEG license or copyright; see Terms of Use at http://library.seg.org/

Downloaded 06/29/16 to 178.250.250.21. Redistribution subject to SEG license or copyright; see Terms of Use at http://library.seg.org/

the portion of the sensitivity near the tool axis changes from strongly negative (Figure 5a) to positive at high dip angles (Figure 5b). Since the tool response is a function of the total sensitivity (represented by both positive and negative sensitivities in Figure 5b), this change in coaxial sensitivity near the tool axis reduces the overall field response. This result also agrees with the coaxial results presented by Wang and Fang (2001) for the same model.

Coplanar simulations are presented in Figure 9 and show contrasting results. One observation from both the horizontal and dipping simulations is that the anisotropic responses differ significantly from the isotropic for the conducting layer between 5 and 8 m (Figure 9a). In particular, the anisotropic response is greater when the layers are horizontal and smaller when the layers are steeply dipping. In this case, some discrepancies exist between our results and those presented by Wang and Fang (2001) for the same model. However, Wang and Fang (2001) present coil-differenced magnetic field results; therefore, a direct comparison with our single-coil simulations is impossible.

Our single-coil results are supported by the sensitivity analysis presented in Figure 5, which shows that the depth sensitivity for the coplanar configuration depends greatly on the anisotropy coefficient and formation dip (Figures 5e–h). In anisotropic formations with 0° dip (Figures 5e and 5f), the coplanar sensitivity is extended to greater distances from the tool axis in the y-plane but remains largely unchanged in the x-plane (the plane containing the formation dip plane) in comparison to the isotropic sensitivity (Figure 5c). The result is an overall increase in the 3D sensitivity in anisotropic formations. If the thin layers are infinite and anisotropic, then the coplanar response is dependent on a greater amount of conductor away from the borehole, resulting in an observed increase in magnetic field response when in the anisotropic layers (Figure 9a). However, if the layers are anisotropic and steeply dipping (Figures 5g and 5h), then the coplanar response is dominated by its sensitivity in the x-plane (Figure 5h). Similar to the coaxial case, the coplanar sensitivity, in this case, is rotated in such a way that the positive and negative lobes interfere to decrease the overall sensitivity and the subsequent response (Figure 9b).

Because layer dip and anisotropy alter the total field amplitude over the isotropic case, assumptions used in inverting multicomponent data for isotropic near-borehole properties can result in error. For example, an isotropic inversion would underestimate (in our coaxial case) the conductivity if the formation were anisotropic and steeply dipping. The magnitude of this error will depend on the magnitude of the conductivity anisotropy coefficient ($\lambda = \sqrt{\sigma_h/\sigma_v}$) and the dip angle of the formation.

Another significant effect of dip is the vertical broadening of the responses as the tool traverses steeply dipping layers. From inspection of Figures 8b and 9b, we see the simulated responses for the 60^o dipping layers clearly are broader in the vertical direction than are the horizontal layer responses. As dip angle increases, the tool senses a progressively thicker conductive section between the horizontal layer boundaries. The result is a field anomaly, which is broader in vertical extent. This effect would not be apparent if the data were plotted as a function of true vertical depth (see Wang and Fang, 2002). Here, we plot the data as a function of distance along the borehole, which increases with increasing dip.

NEAR-BOREHOLE VARIATION EFFECTS

The final simulations examine the interaction of conductive horizontal layers with a borehole and variable-diameter invasion zone and the resulting effect on field responses. This analysis includes results for a 2-m offset tool that traverses a five-layer model. Two scenarios are simulated. The first model contains five isotropic layers of variable conductivity (Figure 2c) with no borehole or invasion zone present. The second model contains the same five layers as before, but a conductive borehole and invasion zone are added (Figure 2d). In this model, the borehole is 0.2 m in diameter with a conductivity of 1 S/m. The invasion zone has a diameter of 0.6 m in the resistive layers and 1.4 m in the conductive layers. The invasion zone is expanded in the conductive layers, assuming that higher conductivity layers have a higher porosity and permeability, allowing for greater invasion of the borehole fluid. The invasion zone conductivity is 0.12 and 0.512 S/m in the resistive and conductive layers, respectively. The results are presented for two source frequencies: 4 and 40 kHz. To determine configuration sensitivity to near-borehole variations, results for the two simulations are compared.

Simulation results

Simulation data are presented in Figure 10 for both five-layer models. Here we compute the total quadrature magnetic field at 0.5-m intervals across the layered model using a fixed source–receiver separation. The results are plotted versus source–receiver midpoint for both the coaxial and coplanar configurations at 4 and 40 kHz. Although it is not necessarily clear from inspection of Figure 10 because of smaller amplitudes at low frequency, the data are equally sensitive to the conductive layers at both 4 and 40 kHz. That is, the percent differences between the two model scenarios are nearly identical at both frequencies simulated. However, the data show a dependence on near-borehole conductivity variations. The model that includes a borehole and invasion produces a larger response, for coaxial and coplanar data, near the conductive layers than does the model without these variations (Figure 10). The separation between the results from the two models is even larger, in some cases, away from the conductive layers.

Percent differences between the coaxial data for the two scenarios are small but range from $\sim$9% to $\sim$19% throughout the model space (Figure 10a). The differences for the coplanar configuration are larger still and range from $\sim$27 to $\sim$100% (excluding extreme values caused by zero crossings in the data). As mentioned, we expect a greater near-borehole response from the coplanar configuration data since this polarization has a sensitivity focused near the tool axis (Figure 5b). Data in Figure 10b show that the discrepancy between the layered response and that of the more realistic borehole model tends to decrease as the tool traverses the resistive layers. The increase in the effect near the thin conductive layers is a result of the expanded invasion zone in those layers as well as the greater conductivity of the invasion zone itself.

Postacquisition processing

Up to this point, we have analyzed the magnitude of the near-borehole effect for various realistic scenarios. We have shown

Downloaded 06/29/16 to 178.250.250.21. Redistribution subject to SEG license or copyright; see Terms of Use at http://library.seg.org/

that the borehole-induced bias can be significant, especially for the coplanar configuration, at short offsets and both high and low frequencies. In this section, we examine a frequency differencing technique by which this bias can be reduced. The method involves measurements made using two frequencies at the same source–receiver offset. Based on formulations presented by Kaufman and Keller (1989) for a two-coil coaxial induction tool, any conducting medium can be divided into two regions: the internal area and the external area. The internal area, which is immediately adjacent to the induction probe, has induced currents that have little influence on current densities in the external area away from the tool axis. The extent of the internal area is determined by source frequency and medium conductivity.

If the induction number is such that the boundary between the internal and external areas is located within the formation, i.e., the near-borehole variations are entirely within the internal area, then the frequency differencing technique can significantly reduce the effect of a borehole (Kaufman and Keller, 1989). For a two-coil coaxial probe operating at different source frequencies, the quadrature component of the magnetic field can be written as

$$QH_z(\omega_1) = \sigma_i\left[\frac{\omega_1\mu T^2}{2}\right] + f(\omega_1, T, \sigma_i), \qquad (4a)$$

$$QH_z(\omega_2) = \sigma_i\left[\frac{\omega_2\mu T^2}{2}\right] + f(\omega_2, T, \sigma_i). \qquad (4b)$$

Here, ω_1 and ω_2 are the source frequencies, σ_i is the frequency-independent apparent conductivity of the internal area when the conductivity of the external area is equal to infinity, T is the probe length, and $f(\omega, T, \sigma_3)$ depends on frequency, probe length, and medium conductivity only. If the current in each receiver coil is equal, then the following function does not depend on the distribution of conductivities in the internal zone:

$$QH_z(FD) = QH_z(\omega_2) - \left[\frac{\omega_2}{\omega_1}\right]QH_z(\omega_1). \qquad (5)$$

Kaufman and Keller (1989) formulated this technique for use with the coaxial configuration; however, we apply it to both the coaxial and coplanar data. Frequency differencing is achieved by applying equation (5) to the total quadrature responses for both five-layer models at 4 and 40 kHz and then comparing the results as in the previous sections.

The differenced total quadrature magnetic field results ($QH_z(FD)$) for both the coaxial and coplanar configurations at 2.0 m offset are shown in Figure 11. When compared with the 40-kHz results in Figure 10, we see the differencing technique has reduced the static shift in the results with and without near-borehole variations. In particular, the coaxial differencing has decreased percent difference values by more than a factor of three. After differencing, the discrepancy between the layered and near-borehole varied models range between −0.4 and 5.0%; however, the thin conductive layer at $z = 0$ is no longer detectable in the coaxial response (Figure 11a).

The reduction in the borehole effect is especially significant for the coplanar fields. The coplanar quadrature field amplitudes cross over zero near the edges of the conductive layers, producing percent difference values that are still measurable; however, the overall difference range is reduced dramatically. In addition to removing most of the borehole effect, frequency

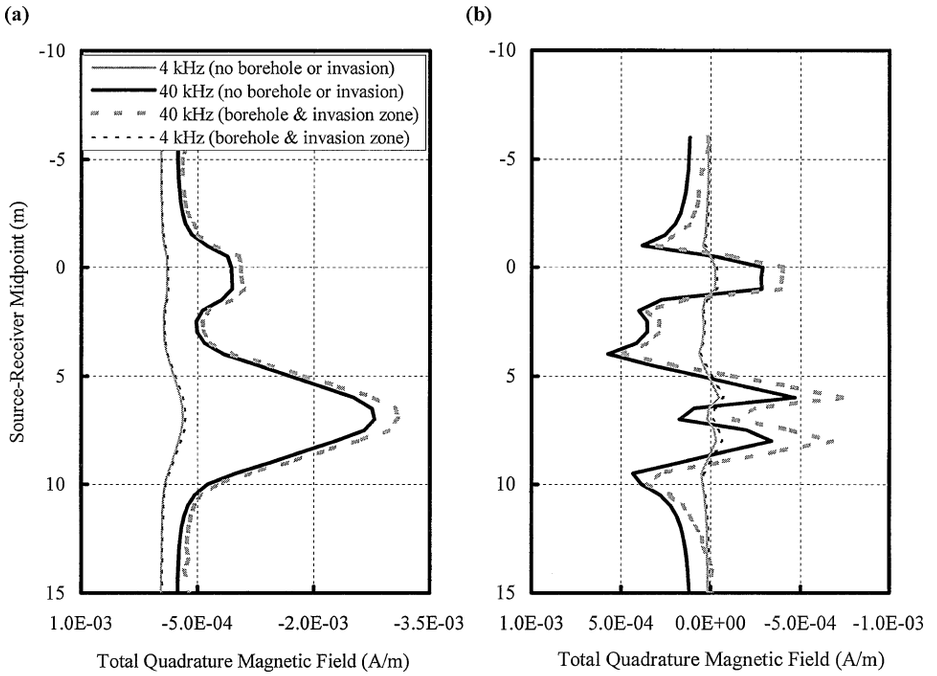

FIG. 10. Coaxial and coplanar responses for the five-layer models shown in Figures 2c and 2d. (a) Response for the five-layer isotropic model at 0° dip for 4- and 40-kHz source frequencies. Results are presented with and without a vertical borehole and invasion zone. (b) Coplanar response for the five-layer model at 0° dip and 4- and 40-kHz source frequencies. Again, results are presented with and without a borehole or invasion present.

Downloaded 06/29/16 to 178.250.250.21. Redistribution subject to SEG license or copyright; see Terms of Use at http://library.seg.org/

differencing reduces the amplitude of the response from the conductive layers, decreasing the signal amplitude by a factor of 2 to 3 for the coaxial configuration and a factor of 5 for the coplanar configuration at 40 kHz. This effect is evident in Figure 11b, where numerical errors in the differenced coplanar solutions are magnified by decreased field amplitudes.

These results suggest that frequency differencing may be effective in removing the borehole-induced bias for the coaxial and coplanar configurations while preserving the integrity of thick layering. A major drawback of frequency differencing, however, is that it reduces sensitivity to thin layers and decreases the amplitude of the measurements. This is evidenced by the obliteration of the coaxial response from the thin conductive layer at $z = 0$ after differencing. The coplanar response to this same layer is maintained after differencing because the field amplitude in this layer is on the order of the largest recorded amplitude.

CONCLUSIONS

We have presented 3D finite-difference simulation results that provide valuable information regarding the behavior of multicomponent induction tools in the presence of anisotropic conducting layers, boreholes, and invasion zones. Coaxial and coplanar tool configurations were simulated, and results indicate that multicomponent magnetic field measurements are affected strongly by tool configurations as well as formation anisotropy and near-borehole conductivity variations.

By simulating multicomponent responses in the presence of thin anisotropic layers, we have shown that the depth sensitivity of multicomponent tools is controlled by source–receiver offset as well as configuration. Our numerical simulations, using finite-length source geometries, substantiate previous findings that fields recorded for coaxial configurations sample a lateral depth of twice the tool offset; however, this distance is reduced to one source–receiver when coplanar source and receiver polarizations are used.

Our simulations also demonstrate that coaxial configurations record identical total field responses for isotropic and anisotropic horizontal layers; however, these configurations record smaller total field amplitudes for anisotropic layers when dip angles are large. In contrast, coplanar configurations record larger total field amplitudes for anisotropic formations at all dip angles.

In addition, we have shown that the coplanar configuration is much more sensitive to a borehole than the coaxial. The influence of the borehole on both components increases with increasing borehole conductivity but is insignificant if the conductivity is less than that of the background. Increasing the borehole diameter also increases the borehole-induced bias.

More realistic model scenarios include effects from both a borehole and invasion zone and demonstrate that these near-borehole variations produce a static shift in the total quadrature responses to conductive layers while preserving the shape of the responses in the absence of these variations. This borehole-induced bias decreases with increasing source–receiver offset and is generally insignificant at 5 m.

To mitigate the borehole-induced bias, we have presented a frequency differencing approach that is effective for both the coaxial and coplanar configurations. This technique reduces the borehole effect yet preserves responses from thick horizontal layers. Unfortunately, frequency differencing significantly reduces signal amplitudes and may completely obliterate the geological signal from thin layers.

ACKNOWLEDGMENTS

This research was performed under the auspices of the Department of Energy's Geothermal Energy Program and the Department of Energy's National Gas and Oil Technology

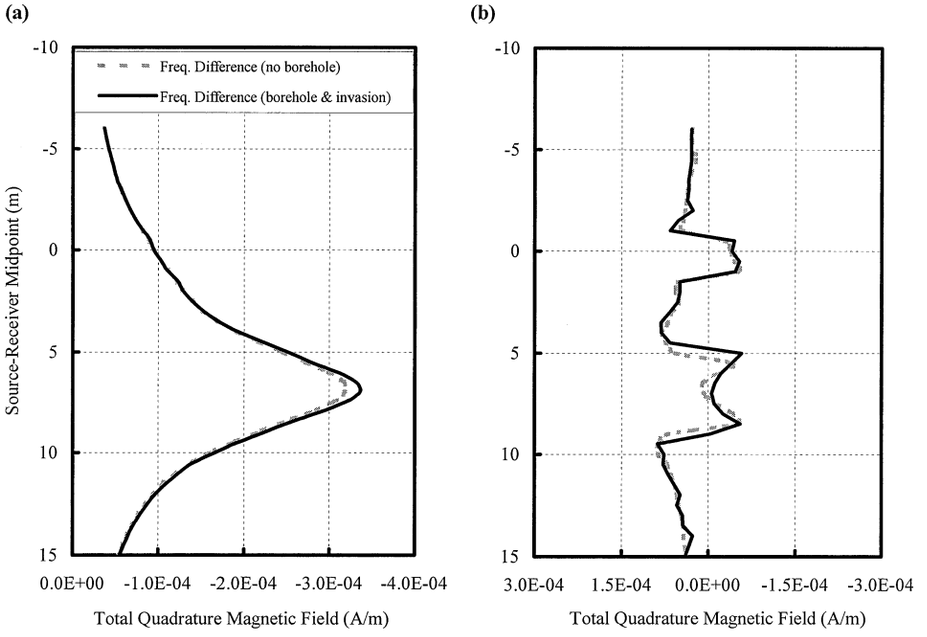

FIG. 11. Coaxial and coplanar responses, after frequency differencing, for the five-layer models shown in Figures 2c and 2d. Quadrature magnetic field data at two frequencies, 4 and 40 kHz, were used for differencing. (a) Coaxial differenced response and (b) coplanar differenced response for the five-layer model at 0° dip with and without a borehole and invasion zone present.

Partnership through Sandia National Laboratories. Industrial sponsors for this project include ExxonMobil, Chevron, Schlumberger–Doll, Baker–Atlas, Halliburton Oilfield Services, KMS Technologies, and Electro-Magnetic Instruments Inc. We thank Kurt Strack of KMS Technologies for suggesting the use of frequency differencing.

REFERENCES

Alumbaugh, D. L., and Wilt, M. J., 1998, 3-D EM imaging from a single borehole: A numerical feasibility study: 68th Annual International Meeting, Society of Exploration Geophysicists, Expanded Abstracts, 448–451.

——— 2001, A numerical sensitivity study of three-dimensional imaging from a single borehole: Petrophysics, **42**, 19–31.

Avdeev, D. B., Kuvshinov, A. V., Pankratov, O. V., and Newman, G. A., 2002, Three-dimensional induction logging problems, part 1: An integral equation solution and model comparisons: Geophysics, **67**, 413–426.

Cheryauka, A. B., Zhdanov, M. S., and Sato, M., 2001, Induction logging with directional coil polarizations: Modeling and resolution analysis: Petrophysics, **42**, 227–236.

Kaufman, A. A., and Keller, G. V., 1989, Induction logging: Methods in geochemistry and geophysics: Elsevier Science Publ. Co., Inc.

Kreigshauser, B., Fanini, O., Yu, L., and Gupta, P., 2000, Advanced inversion techniques for multicomponent induction data: 70th Annual International Meeting, Society of Exploration Geophysicists, Expanded Abstracts, 1810–1813.

Lu, X., and Alumbaugh, D. L., 2001, Three-dimensional sensitivity analysis of induction logging in anisotropic media: Petrophysics, **42**, 566–579.

Moran, J. H., 1982, Induction logging-geometrical factors with skin effect: The Log Analyst, **32**, 4–10.

Newman, G. A., and Alumbaugh, D. L., 1995, Frequency-domain modeling of airborne electromagnetic responses using staggered finite differences: Geophysical Prospecting, **43**, 1021–1042.

——— 2002, Three-dimensional induction logging problems, part 2: A finite-difference solution: Geophysics, **67**, 484–491.

Tompkins, M. J., 2003, Quantitative analysis of multi-component borehole electromagnetic induction responses using anisotropic forward modeling and inversion: Ph.D. dissertation, University of Wisconsin–Madison.

Wang, T., and Fang, S., 2001, 3-D electromagnetic anisotropy modeling using finite differences: Geophysics, **66**, 1386–1398.

Ward, S. H., and Hohmann, G. W., 1988, Electromagnetic theory for geophysical applications, *in* Nabighian, M. N., Ed., Electromagnetic methods in applied geophysics–Theory: Society of Exploration Geophysicists, 131–311.

Yee, K. S., 1966, Numerical solution of initial boundary problems involving Maxwell's equations in isotropic media: IEEE Transactions on Antennas and Propagation, **AP-14**, 302–309.

Downloaded 06/29/16 to 178.250.250.21. Redistribution subject to SEG license or copyright; see Terms of Use at http://library.seg.org/